AIMS Mathematics, 8(5): 11221–11237.
DOI: 10.3934/math.2023568
Received: 01 November 2022
Revised: 24 January 2023
Accepted: 31 January 2023
Published: 09 March 2023

http://www.aimspress.com/journal/Math

Research article

Numerical simulation for thermal enhancement of H_2O + Ethyl Glycol base hybrid nanofluid comprising $GO + (Ag, AA7072, MoS_2)$ nano entities due to a stretched sheet

Yasir Khan[1], Sohaib Abdal[2,3], Sajjad Hussain[4] and Imran Siddique[5,*]

[1] Department of Mathematics, University of Hafr Al Batin, Hafr Al Batin 31991, Saudi Arabia

[2] Department of Mathematics, Khwaja Fareed University of Engineering and Information Technology, Rahim Yar Khan 64200, Pakistan

[3] School of Mathematics, Northwest University, No. 229 North Taibai Avenue, Xi'an 710069, China

[4] School of Aerospace and Mechanical Engineering, Nanyang Technological University, Singapore

[5] Department of Mathematics, University of Management and Technology, Lahore 54770, Pakistan

* **Correspondence:** Email: imransmsrazi@gmail.com; Tel: +923088069883.

Abstract: The evaluation of compact heat density gadgets requires effective measures for heat transportation. Enhancement in thermal transportation of hybrid nanofluids comprising of water plus ethyl glycol with the dispersion of three different nano-entities is considered. The fluids are transported through a porous medium over a permeable elongating sheet. Water and ethyl glycol are $(50\% - 50\%)$. The three cases for hybrid species consist of (a) Graphene oxide (Go) + AA7072, (b) Go + Molybdenum sulfide, (c) Go + silver. The volume fraction of nano-entities is greater than 0.3%. It is presumed that the fluid flow is non-Newtonian. Two on-Newtonian fluids models namely Maxwell fluid and Casson fluid are taken into consideration to present comparative behavior in the existence of the nano-particle mixture. The leading equations are altered into ordinary differential form. A robust numerical procedure embraced with Runge-Kutta methodology and shooting strategy is employed to attain results for the dependent physical quantities. It is noticed that the velocity is diminished against the magnetic field parameter and porosity parameter. The temperature for case (a) Go + AA7072 is the highest and it is lowest for case (c) Go + silver. The temperature and velocity functions of both the fluids (Casson and Maxwell fluids) are incremented with larger inputs of hybrid nano-species. The results can find applications for the better performance of electronic equipment, and heat exchangers.

Keywords: anoparticles; heat source; porous medium; magnetohydrodynamic; Runge-Kutta method
Mathematics Subject Classification: 35Q30, 76D05, 76R10

1. Introduction

Non-Newtonian fluids have recently been revealed to be more adequate for technical and engineering implementations than Newtonian fluids. Such fluids are utilized in a vast scope of engineering and industrial mechanisms, including food manufacturing, metallurgical procedures, the extraction of petroleum goods from crude oil, drilling processes, and bio-engineering procedures. Non-Newtonian liquids encompass viscoelastic liquid, Williamson liquid, Jeffrey liquid, micro polar fluid, power-law liquid, Casson fluid, and others. In 1959, a concept of the Casson fluid [1] is conveyed, which is one of the most significant models for revealing the resources of yield stresses. The connection of fluid and solid stages generates the Casson fluid specimen. When yield stresses are greater than shear stresses, Casson fluid transforms into a solid. Alternatively, it begins to move whenever the yield stresses are fewer than the shear stresses. There are multiple examples like jelly, fruit drinks, beef stew, sauce, tomato, honey, and so on. Human blood can also be thought of as Casson fluid. Salahuddin et al. [2] investigated the stable three-dimensional momentum and inbuilt energy transform in spinning viscous Casson fluid motion with convective boundary situations using the bvp4c technique. Mittal and Patel [3] studied the impacts of thermophoresis, Brownian movement, non-linear heat flux, heat formation and chemical response in a two-dimensional mixed convection flow MHD instability point stream of Casson fluid just beyond a boundless sheet in permeable material numerically utilizing HAM. Likewise, Salahuddin et al. [4], Aneja et al. [5] and Abdal et al. [6] scrutinized the significance of Casson fluid in diverse aspects. Delhibabu et al. [7] discussed MHD 2-D flow flowing between two parallel plates. Ramesh et al. [8] discussed Joule heating and MHD effects on Casson fluid flow by using slip boundary conditions.

Although mono-nanofluids get a stronger thermal system and high rheological assets. Numerous real-time implementations necessitate a trade-off between distinct nanofluid attributes; for instance, metal oxides like Al_2O_3 have beneficial chemical inertia and accuracy but have lesser thermal capacitance whereas metal nanoparticles including copper, aluminum, and gold possess stronger heat conductivity but seem to be chemically reactive and inconsistent. Hybrid nanofluids possess the capability to be used in heat transfer disciplines such as naval formations, microfluidics, defense, health care, acoustic performance, transportation, and so on. There is a wealth of conceptual and experimental results examining hybrid nanofluid attitudes in diverse flowing mechanisms. Muhammad et al. [9] scrutinized the stream of hybrid nano liquid (MWCNTs + Cu + Water), nanofluid (MWCNTs + Water) as well as base liquid (Water) along an arched plate in the existence of viscous dispersion, mixed convection and convective boundary conditions employing the shooting technique and RK-4 methodologies (bvp4c). Souayeh et al. [10] enhanced the heat transfer rate by using hybrid nanoparticles in the presence of activation energy. Mondal et al. [11, 12] used different types of hybrid nano-particles along with a sponge medium to enhance the heat transfer rate of the fluid. Biswas et al. [13] used a partial magnetic field along with hybrid nanoparticles for the convective system in the presence of a porous medium. Mandal et al. [14] used nanofluid thermal transport with a magnetic field in a split-driven porous medium. Mandal et al. [15] investigated the role of bioconvection and MHD for nanofluid flow with sponge medium. Chatterjee et al. [16] studied cooling effects on MHD hybrid nanofluid flow flowing in a cylindrical system. Manna et al. [17] investigated the effects of Lorentz forces on hybrid nanofluid by using entropy generation. Mandal et al. [18] used a non-Darcian porous medium for hybrid nanofluids to improve the heat transfer rate.

A Maxwell fluid is a viscoelastic solid material that may possess both properties of viscosity as well as elasticity. This Maxwell fluid has become the most dominant one in the consideration of researchers as it is the most simple rate-type fluid model. Since Maxwell fluids have less complexity so they play a significant part in the polymeric industry. Aman et al. [19] scrutinized the implication of second-order slip on the magneto-hydrodynamic (MHD) stream of a fractional Maxwell liquid on a moveable sheet as well as the comparative analysis of two numerical methods (Tzou and Stehfest's methodologies). Riaz and Iftikhar [20] utilized fractional-time derivatives to scrutinize the unsteady stream of an MHD Maxwell fluid. Na et al. [21] utilized the Caputo time-fractional derivative to review the free convection stream of Maxwell liquid among two parallel sheets separated by d with dulled shear and heat flux. Shehzad et al. [22] numerically explored the immiscible Maxwell fluid model stream through a spinning disc incorporating thermophoresis as well as the Cattaneo-Christov hypothesis by incorporating Runge-Kutta-4 and shooting technic. Correspondingly, Habib et al. [23], Wang et al. [24], Abdal et al. [25, 26] and Habib et al. [27] reviewed the role of Maxwell fluid flow across the different geometries respectively.

A heat source is anything that can be used to intensify the rate of thermal transition for the desired object from different sources of energy. Heat transfer based on Nanotechnology has transformed our visualization concerning solar systems via Nano-fluids on account of the larger efficacy produced by the adjourned Nano-sized particles. With the passage of time, a method of combustion for solid fuels, which is also a heat source, went hand in hand with humanity's development from the beginning and exploding fire to adjustable, refined, and useful processes. Mahanthesh et al. [28] scrutinized the heat transmission assets of nano-fluid flowing across an elongating revolving disk in the appearance of an imposed gravitational flux and a convective boundary situation. Javed et al. [29] researched the time-dependent fluid motion of Eyring-Powell nanoparticles propelled by a bi-directionally mountable surface encoded in permeable space taking into consideration the thermal and prescribed heat modalities by using the Keller-Box technic. Similarly, Seyednezhad et al. [30], Nielsen et al. [31] and Xiao et al. [32] scrutinized the performance of heat sources in diverse features. Saha et al. [33, 34] enhanced the thermal efficiency and heat transfer rate of practical fluids by using different geometries.

The word boundary layer flow relates to flow in a comparatively shallow region just across a solid substrate at which viscosity has a considerable influence. Prandtl, a German scientist, first proposed the theory of boundary layer flow in 1904. In the present era, the boundary layer is a beneficial feature of engineering owing to its innumerable applications, specifically in the prototype of discrete items to overcome drag forces all through a fluid motion for seamless execution. Ferdows et al. [35] used the bvp4c technic to examine the consequences of radiation, internal temperature formation, and viscous dispersion on the consistent, laminar, immiscible, convective, boundary layer stream of a viscous liquid across a moveable plate. Gangadhar et al. [36] demonstrated an unstable 2-dimensional nanofluid stream of thermal and mass transmission with receding nanoparticle flux. Kebede et al. [37] discussed a computational estimation of the thermal as well as mass transmits attributes of a 2-dimensional time-dependent stream of Williamson nanoparticles across a porous elongating plate inserted in a permeable medium while accounting for the consequences of gravitational flux, heat radiation as well as chemical response utilizing the homotopy analysis method. Berrehal et al. [38] assessed the innate irreversibility of a dissipating water/functionalized carbon nanostructures nanofluid, notably SWCNTs and MWCNTs, in a boundary-layer stream across a convectively warmed moveable

wedge and horizontal/vertical sheets utilizing the shooting technique with the Runge-Kutta-Fehlberg integration strategy. Consequently, Shafee et al. [39], Khan et al. [40] and B. J. et al. [41] viewed distinct performances of boundary layer flow of fluids.

The mechanical and architectural implementations of a boundary layer stream across a consistent stretching surface with energy transmission are remarkable. Such a flow ordinarily comprises wire drafting, glass fiber formation, plastic sheet deformation, hot spinning, conditioning of a metal plate in a conditioning bath, and several mechanisms. Most researchers have examined flow across a sequential elongation of the surface, although there are distinguishing situations in modern and creative methodologies in which the squeezing of the substrate is not typically linear precisely, the flow triggered by a nonlinear flexing sheet performs a crucial task in the polymer extrusion procedure. Reza-E-Rabbi et al. [42] explored the physical implications of the Casson variable, Maxwell factor, heat flux, and viscosity dissipation as well as streamlines and isothermal assessment, on 2D higher-order MHD multiphase liquids stream owing to extending on a flat surface. Ullah et al. [43] utilized Lie group analysis and the shooting methodology to examine the MHD tangent hyperbolic fluid stream over a flexing plate with heat transition attributes and suction/injection influence at the boundary. Ali et al. [44] analyzed the performance of gravitational dipole on the thermal transition phenomena of distinct nano-materials Fe (ferromagnetic) as well as Fe_3O_4 (ferrimagnetic) distributed in a base fluid (60% water + 40% ethylene glycol) on micro-polar liquid stream across a squeezing sheet.

The calibration of hybrid nanofluids has aroused the interest of researchers for heat transfer analysis in recent years. In the previous work [44], nano-particles of iron/iron oxide are utilized, these can cause clogging or rusting. Graphene oxide, MoS_2, and similar nano-particles are harnessed their improved thermal characteristics. Here, various aspects of hybrid nanofluid flow are taken into account which is rarely discussed in existing studies. This work addresses a hybrid base (H_2O + ethyl glycol) where the enhancement in thermal transportation is attained with a homogeneous mixture of three hybrid constituents: (a) $Go + AA7072$, (b) $Go + MoS_2$, (c) $Go + Ag$. These three cases involve vibrant thermo-physical properties as enlisted in Table 1. Two non-Newtonian models are taken into account, these are Casson fluid and Maxwell fluid. Thus a comparative study reveals some interesting results. This work surely augments our understanding of hybrid nanofluid transport phenomena. The findings herein are useful to detect the thermal efficiency of the heat exchangers of heavy industries.

2. Materials and methods

Hybrid nanofluid heat and mass transportation is considered over a stretching sheet that lies along *x-axis*. The fluid is electrically conducting. The sheet is permeable and a magnetic field acts along the y-axis. A porous medium allows the fluid to permeate through. The base fluid is hybrid in the form of water plus ethyl glycol (50% − 50%). Three sets of nano-species namely Graphene oxide plus (a) AA7072, (b) Molybdenum sulfide, (c) silver are separately assumed to be dissolved homogeneously. The concentration of nano solutes is presumed to transform the mixture into non-Newtonian fluids. Two non-Newtonian fluid models are taken for comparative outputs (i) Casson fluids (ii) Maxwell fluids. It is anticipated that the flow is incompressible and velocity components are u, v. The flow passes through a permeable medium and is impacted by a magnetic field along *y-direction*. The flow description of the model is seen in Figure 1. Tables 1 and 2 are shown the thermo-physical properties and characteristics of hybrid base nano-particles. The fluid temperature is T and volume fraction of

Go is ϕ_1 and that of the other additives is ϕ_2. Keeping in consideration, the conservation of mass, momentum, and energy, the physical problem is formulated as below [6, 45].

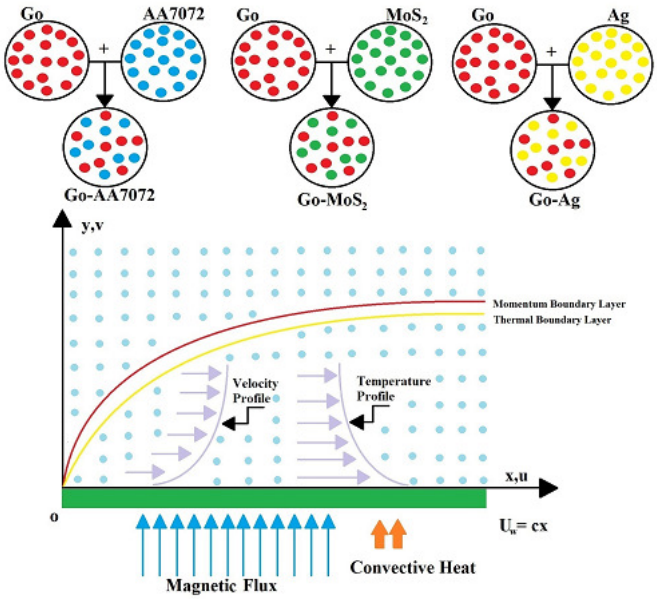

Figure 1. Flow geometry of the problem.

Table 1. Thermo-physical properties of water base fluid and nanoparticles [52–55].

Physical properties	$C_2H_6O_2 - H_2O$	Go	Ag	AA7072	MoS_2
$\rho(kg.m^{-3})$	1063.80	1800	10500	2720	5060
$C_p(J(kg.^\circ k$	3630.00	717	235	893	397
$\kappa(W(m.^\circ k)$	0.378	5000	429	222	904.4

Table 2. Thermo-physical properties of hybrid base fluid and nanoparticles [53, 55, 56].

Properties	Nanofluid	Hybrid Nanofluid
μ(viscosity)	$\mu_{nf} = \frac{\mu_f}{(1-\phi)^{2.5}}$	$\mu_{hnf} = \frac{\mu_f}{(1-\phi_1)^{2.5}(1-\phi_2)^{2.5}}$
ρ(density)	$\rho_{nf} = \rho_f((1-\phi) + \phi\frac{\rho_s}{\rho_f}$	$\rho_{hnf} = \rho_f(1-\phi_2)((1-\phi_1) + \phi_1\frac{\rho_{s1}}{\rho_f}) + \phi_2\rho_{s2}$
ρC_p(Heat capacity)	$(\rho C_p)nf=(\rho C_p)_f((1-\phi)+\phi\frac{(\rho C_p)_s}{(\rho C_p)_f}$	$(\rho C_p)_{hnf}=(\rho C_p)_f(1-\phi_2)((1-\phi_1)+\phi_1\frac{(\rho C_p)_{s1}}{(\rho C_p)_f})+\phi_2(\rho C_p)_{s2}$
κ(Thermal conductivity)	$\frac{\kappa_{nf}}{\kappa_f} = \frac{\kappa_s+(s_f-1)\kappa_f-(s_f-1)\phi(\kappa_f-\kappa_s)}{\kappa_s+(s_f-1)\kappa_f+\phi(\kappa_f-\kappa_s)}$	$\frac{\kappa_{hnf}}{\kappa_{bf}} = \frac{\kappa_{s2}+(s_f-1)\kappa_{bf}-(s_f-1)\phi_2(\kappa_{bf}-\kappa_{s2})}{\kappa_{s2}+(s_f-1)\kappa_{bf}+\phi(\kappa_{bf}-\kappa_{s2})}$ where $\frac{\kappa_{bf}}{\kappa_f} = \frac{\kappa_{s1}+(s_f-1)\kappa_f-(s_f-1)\phi_1(\kappa_f-\kappa_{s1})}{\kappa_{s1}+(s_f-1)\kappa_f+\phi(\kappa_f-\kappa_{s1})}$
σ(Electrical conductivity)	$\frac{\sigma_{nf}}{\sigma_f} = 1 + \frac{3(\sigma-1)\phi}{(\sigma+2)-(\sigma-1)\phi}$	$\frac{\sigma_{hnf}}{\sigma_{bf}} = 1 + \frac{3\phi(\sigma_1\phi_1+\sigma_2\phi_2-\sigma_{bf}(\phi_1+\phi_2))}{(\sigma_1\phi_1+\sigma_2\phi_2+2\phi\sigma_{bf})-\phi\sigma_{bf}((\sigma_1\phi_1+\sigma_2\phi_2)-\sigma_{bf}(\phi_1+\phi_2))}$

Governing equations

$$\frac{\partial u}{\partial x} + \frac{\partial v}{\partial y} = 0, \tag{2.1}$$

$$u\frac{\partial u}{\partial x}+v\frac{\partial u}{\partial y}=\frac{\mu_{hnf}}{\rho_{hnf}}\left(1+\frac{1}{\beta}\right)\frac{\partial^2 u}{\partial y^2}-\frac{\sigma B_0^2 u}{\rho_{hnf}}-\frac{\mu_{hnf}}{\rho_{hnf}}\frac{u}{k^*}-\lambda_M\left[u^2\frac{\partial^2 u}{\partial x^2}+v^2\frac{\partial^2 u}{\partial y^2}+2uv\frac{\partial^2 u}{\partial y\partial x}\right], \tag{2.2}$$

$$u\frac{\partial T}{\partial x}+v\frac{\partial T}{\partial y}=\frac{k_{hnf}}{(\rho C_p)_{hnf}}\frac{\partial^2 T}{\partial y^2}+\frac{\mu_{hnf}}{(\rho C_p)_{hnf}}\left(\frac{\partial u}{\partial x}\right)^2+\frac{Q_0}{(\rho C_p)_{hnf}}(T-T_\infty). \tag{2.3}$$

The supportive boundary conditions are:

$$\left.\begin{aligned}u-U_w=cx=0, v-v_w=0, T-T_w(x)=0,\ as\ y=0,\\ u\to 0,\ T\to T_\infty,\ as\ y\to\infty.\end{aligned}\right\} \tag{2.4}$$

The uniform velocity at wall is v_w (where, $v_w<0$ for suction, $v_w>0$ for injection), h_f is heat transition coefficient, Employing the similarity factors:

$$\left.\begin{aligned}u=u_w=u_o(x+y)^m,\ v=0,\ T=T_w,\ C=C_w,\ \textbf{at}\ y=B(x+b)^{\frac{1-m}{2}}\\ u\longrightarrow 0,\ T\longrightarrow T_\infty,\ C\longrightarrow C_\infty,\ \textbf{when}\ y\longrightarrow\infty\end{aligned}\right\} \tag{2.5}$$

$$\left(1+\frac{1}{\beta}\right)f'''-A_1(f'^2-ff'')-A_2Mf'-K_pf'+\lambda A_1(f^2f'''-2ff'f'')=0, \tag{2.6}$$

$$\theta''-\frac{k_f}{k_{hnf}}Pr(A_3f\theta'-EcA_4f''^2-Q\theta)=0, \tag{2.7}$$

$$\left.\begin{aligned}f(\eta)-S=0,\ f'(\eta)-1=0,\ \frac{k_{hnf}}{k_f}\theta'(\eta)-B_i(1-\theta(\eta))=0,\ at\ \eta=0,\\ f'(\infty)\to 0,\ \theta(\infty)\to 0,\ as\ \eta\to\infty.\end{aligned}\right\} \tag{2.8}$$

where magnetic factor is M, porosity factor is K_p, Maxwell Deborah number is λ, Pr is Prandtl number, Eckert number is Ec, heat source is Q, suction factor is S and Biot number is B_i.

$$M=\frac{\sigma B_o^2}{\rho_f c},\ K_p=\frac{\nu_f}{ck^*},\ \lambda=\lambda_M c,\ Pr=\frac{\nu_f(\rho C_p)_f}{\kappa_f},$$
$$Ec=\frac{c^2x^2}{(C_p)_f(T_w-T_\infty)},\ Q=\frac{Q_0}{c(\rho C_p)_{hnf}},$$
$$S=\frac{v_w}{\sqrt{c\nu_f}},\ B_i=\frac{h}{k_f}\sqrt{\frac{\nu_f}{c}}.$$

Also

$$A_1=(1-\phi_1)^{2.5}(1-\phi_2)^{2.5}[(1-\phi_2)\left\{(1-\phi_1)+\phi_1\frac{\rho_{s1}}{\rho_f}\right\}+\phi_2\frac{\rho_{s2}}{\rho_f}],$$
$$A_2=(1-\phi_2)\left\{(1-\phi_1)+\phi_1\frac{\rho_{s1}}{\rho_f}\right\}+\phi_2\frac{\rho_{s2}}{\rho_f},$$
$$A_3=(1-\phi_2)\left\{(1-\phi_1)+\phi_1\frac{(\rho C_p)_{s1}}{(\rho C_p)_f}\right\}+\phi_2\frac{(\rho C_p)_{s2}}{(\rho C_p)_f},$$
$$A_4=(1-\phi_1)^{2.5}(1-\phi_2)^{2.5},$$

$$\frac{k_{hnf}}{k_f} = \frac{\kappa_{s2} + (s_f - 1)\kappa_{bf} - (s_f - 1)\phi_2(\kappa_{bf} - \kappa_{s2})}{\kappa_{s2} + (s_f - 1)\kappa_{bf} + \phi_2(\kappa_{bf} - \kappa_{s2})}.\frac{\kappa_{s1} + (s_f - 1)\kappa_f - (s_f - 1)\phi_1(\kappa_f - \kappa_{s1})}{\kappa_{s1} + (s_f - 1)\kappa_f + \Phi_1(\kappa_f - \kappa_{s1})}.$$

The interpretations for skin friction correlation and the local Nusselt number are as follows (see [46, 47]):

$$C_f = \frac{\tau_w}{\rho_f U_w^2},\ Nu = \frac{xq_w}{k_f(T_w - T_\infty)}, \tau_w = \mu_{hnf}(1 + \frac{1}{\beta})(\frac{\partial u}{\partial y})(forCassonfluid),$$
$$\tau_w = \mu_{hnf}(1 + \lambda_M)(\frac{\partial u}{\partial y})(forMaxwellfluid),\ q_w = k_{hnf}\frac{\partial T}{\partial y},\ at\ y = 0. \tag{2.9}$$

By employing the similarity transformation equation, we acquire

$$\begin{cases} Cf_x {Re_x}^{1/2} = (1 + \frac{1}{\beta})\frac{f''(0)}{A_4}, (forCassonfluid), \\ Cf_x {Re_x}^{1/2} = (1 + \lambda)\frac{f''(0)}{A_4}, (forMaxwellfluid), \\ Nu_x {Re_x}^{-1/2} = -\frac{\left[k_{hnf}\theta'(0)\right]}{k_f}. \end{cases} \tag{2.10}$$

Solution procedure

The mathematical formulation as finally constructed in the form of a boundary value problem (Eqs (6)–(8)) contains non-linear terms and up to third-order derivatives are involved. As usual, it is cumbersome to attain any closed-form solutions for this BVP. Numerical treatment based on the RK-4 method with shooting technique as operated by [48–51] is hired to yield a solution to the problem. The basic layout of the scheme is to convert the derivatives of high order into order first derivatives as given below:

$s_1' = s_2$

$s_2' = s_3$

$(1 + 1/\beta)s_3' = A_1(s_2^2 - s_1 s_3) + A_2 M s_2 + K_p s_2 + \lambda A_1(S_1^2 s_3' - 2s_1 s_2 s_3)$

$s_4' = s_5$

$s_5' = \frac{k_f}{k_{hnf}} Pr(A_3 s_1 s_5 - EcA_4 s_3^2 - Q s_4)$

along with the boundary conditions:

$s_1 = S,\ s_2 = 1, \frac{k_{hnf}}{k_f} s_5 = B_i(1 - s_4)$, at $\eta = 0$

$s_2 \to 0,\ s_4 \to 0\ as\ \eta \to \infty$. This system of first-ordered differential equations makes a two-point boundary value problem. The coding of the numerical scheme is developd and rises in the Matlab environment. The commercial software Matlab R2018b is licensed at the non-linear center of studies, Northwest west university, Xian, China. The maximum value of $\eta \to \infty$ is replaced by $\eta_{max} = 6$.

3. Results and discussions

This portion pertains to the presentation and interpretation of momentum and heat distribution for the three cases of hybrid nanofluid dynamics owing to a stretching surface. Parametric deliberation grows from the computational procedure as described in the above section. Prior to the evaluation of

current results, limiting values of the parameters are used to validate the code. The values of the Nusselt number enlisted in Table 3 show reasonable agreement among themselves to ensure the validity of the current numerical procedure. Then, results for the notable physical variables are evaluated for opposite ranges of the pertinent parameters namely magnetic field (M), the porosity of medium (K_p), Maxwell fluid (λ), Casson fluid (β), mass suction (S) and heat source (Q). Table 4 indicates that magnitude of skin friction is enhanced directly with higher inputs of M, λ, K_p, and S but it is reduced against parameter β. Further, the skin friction is largest for hybrid species case (a) $Go + AA7072$ and it is smallest for case (c) $Go + Ag$. From Table 5, the behavior of the Nusselt number convinced that the local heat transfer is enhanced with Pr but it diminishes against Ec and Q. From Table 6, it is seen that $-\theta'(0)$ is highest for case (c) $Go + Ag$ and it is lowest for case (a) $Go + AA7072$.

Table 3. Comparative outputs for Pr when the rest factors are zeros.

Pr	Gorla and Sidawi [57]	Khan and Pop [58]	Wang [59]	Devi et al. [60]	Our results
2.0	0.9114	0.9113	0.9114	0.91135	0.9113
6.13	–	–	–	1.75968	1.7596
2.0	1.8954	1.8954	1.8954	1.89540	1.8954
20.0	3.3539	3.3539	3.3539	3.35390	3.3539

Table 4. Findings for Skin friction factor $-f''(0)$ for Casson fluid.

M	K_p	β	S	$Go + AA7072$	$Go + MoS_2$	$Go + Ag$
0.0	0.5	1.0	0.5	2.2987	2.2712	2.2108
0.5				2.6317	2.6008	2.5328
1.0				2.9232	2.8893	2.8146
0.5	0.1			2.3962	2.3677	2.3050
	0.3			2.5170	2.4873	2.4219
	0.5			2.6317	2.6008	2.5328
	0.1	0.5		3.1498	3.1136	3.0339
		1.0		2.6317	2.6008	2.5328
		1.5		2.4315	2.4027	2.3392
		1.0	0.1	2.3774	2.3519	2.2958
			0.3	2.5016	2.4735	2.4116
			0.5	2.6317	2.6008	2.5328

Table 5. Findings for Skin friction factor $-f''(0)$ for Maxwell fluid.

M	K_p	λ	S	$Go + AA7072$	$Go + MoS_2$	$Go + Ag$
0.0	0.5	0.5	0.5	2.4738	2.4659	2.4474
0.5				2.7993	2.7913	2.7728
1.0				3.0823	3.0743	3.0556
0.5	0.1			2.5695	2.5615	2.5430
	0.3			2.6876	2.6796	2.6611
	0.5			2.7993	2.7913	2.7728
	0.1	0.5		2.7993	2.7919	2.7728
		1.0		3.6939	3.6747	3.6308
		1.5		4.5719	4.5393	4.4651
		0.5	0.1	2.5265	2.5247	2.5206
			0.3	2.6945	2.6902	2.6802
			0.5	2.7993	2.7913	2.7728

Table 6. Findings for Nusselt number $-\theta'(0)$.

Pr	Ec	Q	$Go + AA7072$	$Go + MoS_2$	$Go + Ag$
6.135	0.1	0.01	0.5447	0.5460	0.5488
7.0			0.5653	0.5666	0.5696
8.0			0.5854	0.5868	0.5899
6.135	0.01		0.6255	0.6257	0.6262
	0.05		0.5896	0.5903	0.5918
	0.1		0.5447	0.5460	0.5488
	0.1	0.01	0.5447	0.5460	0.5488
		0.02	0.5420	0.5434	0.5462
		0.03	0.5393	0.5406	0.5435

Figures 2–7 are plotted for velocity and temperature distribution for three cases of hybrid nanofluid namely (a) $Go + AA7072$ / hybrid base, (b) $Go + MoS_2$ / hybrid base, (c) $Go + Ag$ / hybrid base. For the plots of Figure 2(a), it readily comes to know that the flow speed $f'(\eta)$ declines against magnetic field strength M (see [56]). Actually, greater values of M cross pond to reduce larger resistive force (Lorentz force) because magnetic and electric fields intervene. Similarly in Figure 2(b), the velocity curves slope down against larger values of K_p (porosity parameter). The larger K_p means lesser permeability of the medium that offers increased resistance to the motion and hence the speed reduction (see [53]). Figure 3(a) depicts the impact of Casson factor β on $f'(\eta)$. It is revealed that the speed of the fluid decelerates when the nature of fluid transform from Casson fluid to Newtonian fluid (β enhances). The larger values of the Maxwell parameter enhance flow speed as depicted in Figure 3(b). The implications of suction/injection factor S on the flow velocity $f'(\eta)$ are mapped in Figure 3(c). The flow becomes faster for injection ($S < 0$) and it is slowed down against suction ($S > 0$). Figure 4(a),(b) respectively show the impacts of volume fraction ϕ_2 on the fluid velocity for the Casson model and Maxwell model. It is seen that the velocity $f'(\eta)$ goes down with increments in ϕ_2. Further, Figures 2 to 4 indicate that the velocity of the hybrid nanofluid is faster for case (a) $Go + AA7072$ and it is slower for case (c) $Go + Ag$. Figure 5(a),(b), graphs are drawn respectively for fluids temperature $\theta(\eta)$ for the Casson fluid and Maxwell fluid. The fluid temperature $\theta(\eta)$ is incremented with a rise in the volume fraction ϕ_2 of nano-species. As seen from Figure 6(a), the hybrid nanofluids temperature is decreased against the higher valuation of Prandtl number Pr. The higher Prandtl number means the lesser heat diffusivity. The fluid's temperature rises with increasing strengths of heat source factor Q as well as Eckert number Ec as noticed respectively in Figures 6(b) and 7(a) (see [55]). The growing values of Biot number B_i also enhance the temperature of the fluid as seen in Figure 7(b). Moreover, fluids temperature for hybrid nanofluid case (a) $Go + AA7072$ remains the highest whereas it is smallest for the case (c) $Go + Ag$.

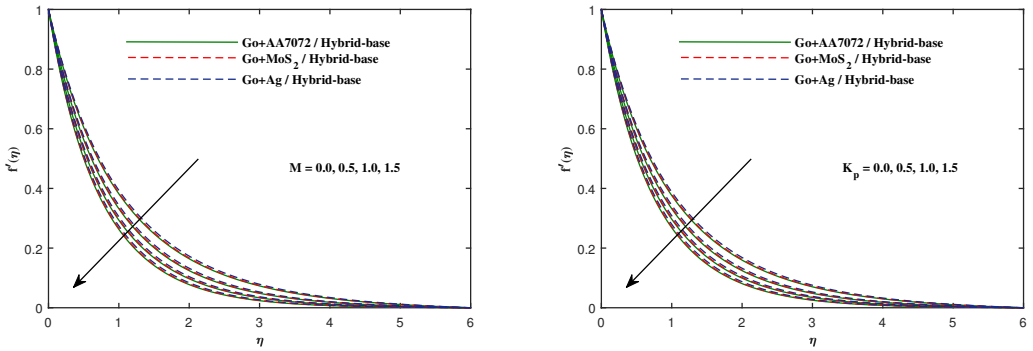

Figure 2. Fluctuation of $f'(\eta)$ along with (a) M and (b) K_p.

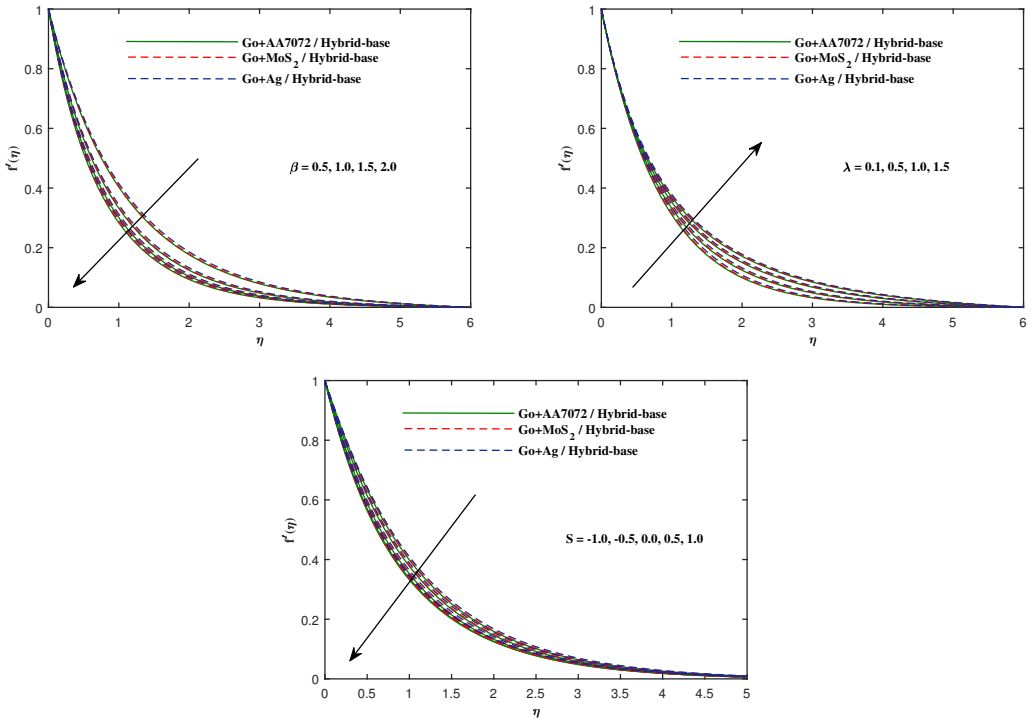

Figure 3. Fluctuation of $f'(\eta)$ along with (a) β, (b) λ and (c) S.

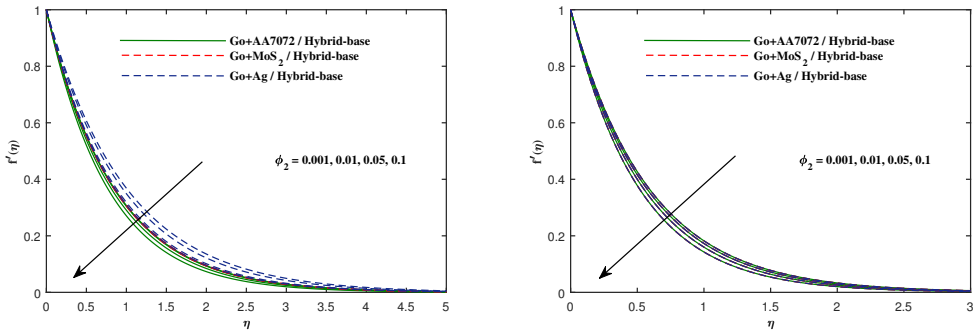

Figure 4. Fluctuation of $f'(\eta)$ along with ϕ_2 (a) Casson fluid β and (b) Maxwell fluid λ.

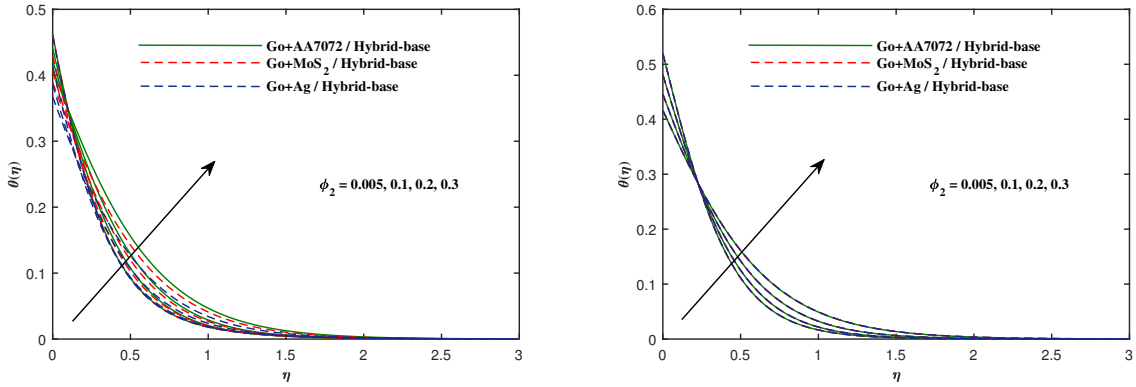

Figure 5. Fluctuation of $\theta(\eta)$ along with ϕ_2 (a) Casson fluid β and (b) Maxwell fluid λ.

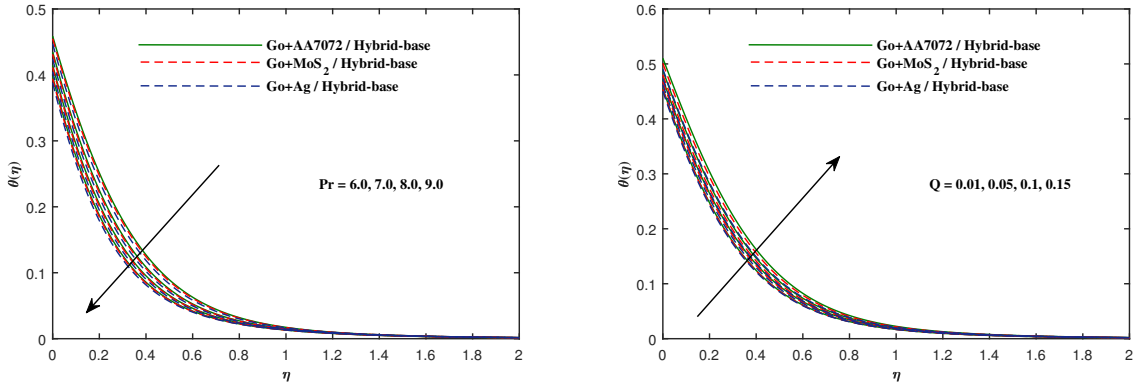

Figure 6. Fluctuation of $\theta(\eta)$ along with (a) Pr and (b) Q.

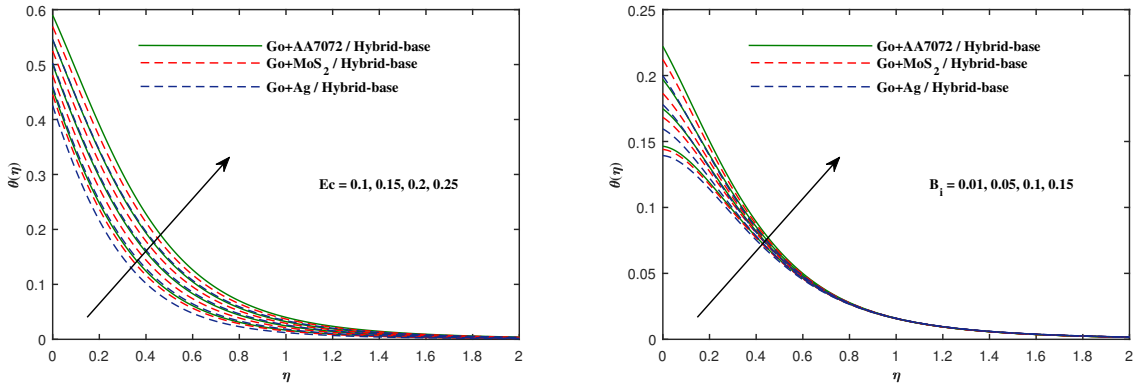

Figure 7. Fluctuation of $\theta(\eta)$ along with (a) Ec and (b) B_i.

4. Conclusions

The central point of this work is the consideration of hybrid base hybrid nanofluid transportation across a stretching sheet. The bulk fluid is a homogeneous mixture of (50% − 50%) water + ethyl glycol. Three hybrid nano-species: Silver, Molybdenum sulfide, and AA7072 are taken separately with Graphene oxide. These blends of nano-materials are mixed in hybrid base fluids. A detailed analysis of the practical designs are presented to elucidate the flow and heat transportation pertaining to the enhanced thermal efficiency of heat exchangers. The fluid flow models namely Casson fluid and Maxwell fluid are theoretically considered for non-Newtonian behavior of the nanofluids with concentration greater than 0.03 %. Numerical outcomes are briefly defined below:

- Velocity $f'(\eta)$ goes down against the upsurge values of magnetic factor M, K_p, β as well as S.
- Elevated Maxwell fluid factor λ inputs explicitly upsurge velocity $f'(\eta)$.
- With the up surged values of volume fraction ϕ_2, the fluid velocity for the Casson model and Maxwell model shows decreasing behavior.
- It is noted that when Pr is uplifted, temperature $\theta(\eta)$ goes down.
- Temperature $\theta(\eta)$ rises rapidly when Q, Ec and B_i takes larger values.
- It is interesting to note that temperature $\theta(\eta)$ increases quickly for both the fluid models when ϕ_2 takes higher inputs.
- For Casson fluid model, skin friction coefficient boosted with M, S and K_p but with the developing values of β induce for reduction of $-f''(0)$.
- With the higher inputs of Prandtl number, $-\theta'(0)$ uplifted while opposite behavior observed for Q, Bi and Eckert number Ec.

Acknowledgments

This research work was funded by institutional fund projects under no. (IFP-A- 2022-2-5-24). Therefore, the authors gratefully acknowledge technical and financial support from the ministry of education and the University of Hafr Al Batin, Saudi Arabia.

Conflict of interest

The authors declare no conflict of interest.

References

1. N. Casson, A flow equation for pigment-oil suspensions of the printing ink type, *Rheol. Disperse Syst.*, 1959.
2. T. Salahuddin, M. Arshad, N. Siddique, A. Alqahtani, M. Malik, Thermophyical properties and internal energy change in Casson fluid flow along with activation energy, *Ain Shams Eng. J.*, **11** (2020), 1355–1365. https://doi.org/10.1016/j.asej.2020.02.011
3. A. S. Mittal, H. R. Patel, Influence of thermophoresis and brownian motion on mixed convection two dimensional MHD Casson fluid flow with non-linear radiation and heat generation, *Physica A*, **537** (2020), 122710. https://doi.org/10.1016/j.physa.2019.122710

4. T. Salahuddin, N. Siddique, M. Arshad, I. Tlili, Internal energy change and activation energy effects on Casson fluid, *AIP Adv.*, **10** (2020), 025009. https://doi.org/10.1016/10.1063/1.5140349

5. M. Aneja, A. Chandra, S. Sharma, Natural convection in a partially heated porous cavity to Casson fluid, *Int. Commun. Heat Mass*, **114** (2020), 104555. https://doi.org/10.1016/j.icheatmasstransfer.2020.104555

6. S. Abdal, S. Hussain, I. Siddique, A. Ahmadian, M. Ferrara, On solution existence of MHD Casson nanofluid transportation across an extending cylinder through porous media and evaluation of priori bounds, *Sci. Rep.*, **11** (2021), 1–16. https://doi.org/10.20944/preprints202012.0168.v1

7. R. Delhibabu, V. Yuvaraj, J. A. Nisha, K. K. Vendhan, *Analytical study of steady magneto hydrodynamic two-dimensional flow between parallel porous plates with an angular velocity to an inclined magnetic field*, In: AIP Conf. Proc., **2464** (2022), AIP Publishing LLC, 050001.

8. K. Ramesh, A. Riaz, Z. A. Dar, Simultaneous effects of mhd and joule heating on the fundamental flows of a Casson liquid with slip boundaries, *Propuls. Power Res.*, **10** (2021), 118–129. https://doi.org/10.1016/j.jppr.2021.05.002

9. K. Muhammad, T. Hayat, A. Alsaedi, B. Ahmad, S. Momani, Mixed convective slip flow of hybrid nanofluid (MWCNTs+ Cu+ Water), nanofluid (MWCNTs+ Water) and base fluid (Water): A comparative investigation, *J. Therma. Anal. Calorim.*, **143** (2021), 1523–1536. https://doi.org/10.1007/s10973-020-09577-z

10. B. Souayeh, K. Ramesh, N. Hdhiri, E. Yasin, M. W. Alam, K. Alfares, A. Yasin, Heat transfer attributes of gold-silver-blood hybrid nanomaterial flow in an emhd peristaltic channel with activation energy, *Nanomaterials*, **12** (2022), 1615.

11. D. K. Mandal, N. Biswas, N. K. Manna, R. S. R. Gorla, A. J. Chamkha, Magneto-hydrothermal performance of hybrid nanofluid flow through a non-darcian porous complex wavy enclosure, *Eur. Phys. J. Spec. Top.*, 2022, 1–18.

12. M. K. Mondal, N. Biswas, A. Datta, B. K. Sarkar, N. K. Manna, Positional impacts of partial wall translations on hybrid nanofluid flow in porous media: Real Coded Genetic Algorithm (RCGA), *Int. J. Mech. Sci.*, **217** (2022), 107030. https://doi.org/10.1016/j.ijmecsci.2021.107030

13. N. Biswas, M. K. Mondal, N. K. Manna, D. K. Mandal, A. J. Chamkha, Implementation of partial magnetic fields to magneto-thermal convective systems operated using hybrid-nanoliquid and porous media, *P. I. Mech. Eng. C-J. Mech.*, **236** (2022), 5687–5704. https://doi.org/10.1177/09544062211060168

14. D. K. Mandal, M. K. Mondal, N. Biswas, N. K. Manna, R. S. R. Gorla, A. J. Chamkha, Nanofluidic thermal-fluid transport in a split-driven porous system working under a magnetic environment, *Int. J. Numer. Method. H.*, **32** (2021), 1–14. https://doi.org/10.1108/HFF-08-2021-0555

15. D. K. Mandal, N. Biswas, N. K. Manna, R. S. R. Gorla, A. J. Chamkha, Role of surface undulation during mixed bioconvective nanofluid flow in porous media in presence of oxytactic bacteria and magnetic fields, *Int. J. Mech. Sci.*, **211** (2021), 106778.

16. D. Chatterjee, N. Biswas, N. K. Manna, S. Sarkar, Effect of discrete heating-cooling on magneto-thermal-hybrid nanofluidic convection in cylindrical system, *Int. J. Mech. Sci.*, **238** (2023), 107852.

17. N. K. Manna, N. Biswas, D. K. Mandal, U. Sarkar, H. F. Öztop, N. Abu-Hamdeh, Impacts of heater-cooler position and lorentz force on heat transfer and entropy generation of hybrid nanofluid convection in quarter-circular cavity, *Int. J. Numer. Method. H.*, 2022.

18. D. K. Mandal, N. Biswas, N. K. Manna, D. K. Gayen, R. S. R. Gorla, A. J. Chamkha, Thermo-fluidic transport process in a novel M-shaped cavity packed with non-Darcian porous medium and hybrid nanofluid: Application of artificial neural network (ANN), *Phys. Fluids*, **34** (2022), 033608. https://doi.org/10.1063/5.0082942

19. S. Aman, Q. Al-Mdallal, I. Khan, Heat transfer and second order slip effect on MHD flow of fractional maxwell fluid in a porous medium, *J. King Saud Unive. Sci.*, **32** (2020), 450–458. https://doi.org/10.1016/j.jksus.2018.07.007

20. M. Riaz, N. Iftikhar, A comparative study of heat transfer analysis of MHD maxwell fluid in view of local and nonlocal differential operators, *Chaos Soliton. Fract.*, **132** (2020), 109556. https://doi.org/10.1016/j.chaos.2019.109556

21. W. Na, N. A. Shah, I. Tlili, I. Siddique, Maxwell fluid flow between vertical plates with damped shear and thermal flux: Free convection, *Chinese J. Phys.*, **65** (2020), 367–376. https://doi.org/10.1016/j.cjph.2020.03.005

22. S. Shehzad, F. Mabood, A. Rauf, I. Tlili, Forced convective maxwell fluid flow through rotating disk under the thermophoretic particles motion, *Int. Commun. Heat Mass*, **116** (2020), 104693. https://doi.org/10.1016/j.icheatmasstransfer.2020.104693

23. D. Habib, N. Salamat, M. Ahsan, S. Abdal, I. Siddique, B. Ali, Significance of bioconvection and mass transpiration for mhd micropolar maxwell nanofluid flow over an extending sheet, *Wave. Random Complex*, 2022, 1–15.

24. W. Wang, M. M. Jaradat, I. Siddique, A. A. A. Mousa, S. Abdal, Z. Mustafa, et al., On thermal distribution for darcy-forchheimer flow of maxwell sutterby nanofluids over a radiated extending surface, *Nanomaterials*, **12** (2022), 1834. https://doi.org/10.3390/nano12111834

25. S. Abdal, I. Siddique, A. Ahmadian, S. Salahshour, M. Salimi, Enhanced heat transportation for bioconvective motion of maxwell nanofluids over a stretching sheet with Cattaneo-Christov flux, *Mechanics Time-Depend. Mat.*, 2022, 1–16.

26. S. Abdal, I. Siddique, D. Alrowaili, Q. Al-Mdallal, S. Hussain, Exploring the magnetohydrodynamic stretched flow of williamson maxwell nanofluid through porous matrix over a permeated sheet with bioconvection and activation energy, *Sci. Rep.*, **12** (2022), 1–12.

27. U. Habib, S. Abdal, I. Siddique, R. Ali, A comparative study on micropolar, williamson, maxwell nanofluids flow due to a stretching surface in the presence of bioconvection, double diffusion and activation energy, *Int. Commun. Heat Mass*, **127** (2021), 105551. https://doi.org/10.1016/j.icheatmasstransfer.2021.105551

28. B. Mahanthesh, N. S. Shashikumar, G. Lorenzini, Heat transfer enhancement due to nanoparticles, magnetic field, thermal and exponential space-dependent heat source aspects in nanoliquid flow past a stretchable spinning disk, *J. Therm. Anal. Calorim.*, 2020, 1–9.

29. T. Javed, M. Faisal, I. Ahmad, Dynamisms of solar radiation and prescribed heat sources on bidirectional flow of magnetized eyring-powell nanofluid, *Case Stud. Therm. Eng.*, **21** (2020), 100689. https://doi.org/10.1016/j.csite.2020.100689

30. M. Seyednezhad, M. Sheikholeslami, J. A. Ali, A. Shafee, T. K. Nguyen, Nanoparticles for water desalination in solar heat exchanger, *J. Therm. Anal. Calorim.*, **139** (2020), 1619–1636. https://doi.org/10.1007/s10973-019-08634-6

31. S. Nielsen, K. Hansen, R. Lund, D. Moreno, Unconventional excess heat sources for district heating in a national energy system context, *Energies*, **13** (2020), 5068. https://doi.org/10.3390/en13195068

32. B. Xiao, W. Deng, Z. Ma, S. He, L. He, X. Li, et al., Experimental investigation of loop heat pipe with a large squared evaporator for multi-heat sources cooling, *Renew. Energ.*, **147** (2020), 239–248. https://doi.org/10.1016/j.renene.2019.08.142

33. A. Saha, A. Chakravarty, K. Ghosh, N. Biswas, N. K. Manna, Role of obstructing block on enhanced heat transfer in a concentric annulus, *Wave. Random Complex*, 2022, 1–25.

34. A. Saha, N. K. Manna, K. Ghosh, N. Biswas, Analysis of geometrical shape impact on thermal management of practical fluids using square and circular cavities, *Eur. Phys. J. Spec. Top.*, 2022, 1–29.

35. M. Ferdows, M. Shamshuddin, S. Salawu, K. Zaimi, Numerical simulation for the steady nanofluid boundary layer flow over a moving plate with suction and heat generation, *SN Appl. Sci.*, **3** (2021), 1–11. https://doi.org/10.1007/s42452-021-04224-0

36. K. Gangadhar, T. Kannan, G. Sakthivel, K. DasaradhaRamaiah, Unsteady free convective boundary layer flow of a nanofluid past a stretching surface using a spectral relaxation method, *Int. J. Ambient Energy*, **41** (2020), 609–616. https://doi.org/10.1080/01430750.2018.1472648

37. T. Kebede, E. Haile, G. Awgichew, T. Walelign, Heat and mass transfer in unsteady boundary layer flow of williamson nanofluids, *J. Appl. Math.*, **2020** (2020). https://doi.org/10.1155/2020/1890972

38. H. Berrehal, F. Mabood, O. Makinde, Entropy-optimized radiating water/FCNTs nanofluid boundary-layer flow with convective condition, *Eur. Phys. J. Plus*, **135** (2020), 1–21.

39. A. Shafee, M. Sheikholeslami, M. Jafaryar, H. Babazadeh, Hybrid nanoparticle swirl flow due to presence of turbulator within a tube, *J. Therm. Anal. Calorim.*, **144** (2021), 983–991.

40. U. Khan, A. Zaib, Z. Shah, D. Baleanu, E. S. M. Sherif, Impact of magnetic field on boundary-layer flow of Sisko liquid comprising nanomaterials migration through radially shrinking/stretching surface with zero mass flux, *J. Mater. Res. Technol.*, **9** (2020), 3699–3709.

41. B. Gireesha, M. Umeshaiah, B. Prasannakumara, N. Shashikumar, M. Archana, Impact of nonlinear thermal radiation on magnetohydrodynamic three dimensional boundary layer flow of jeffrey nanofluid over a nonlinearly permeable stretching sheet, *Physica A*, **549** (2020), 124051. https://doi.org/10.1016/j.physa.2019.124051

42. S. Reza-E-Rabbi, S. F. Ahmmed, S. Arifuzzaman, T. Sarkar, M. S. Khan, Computational modelling of multiphase fluid flow behaviour over a stretching sheet in the presence of nanoparticles, *Eng. Sci. Technol.*, **23** (2020), 605–617. https://doi.org/10.1016/J.JESTCH.2019.07.006

43. Z. Ullah, G. Zaman, A. Ishak, Magnetohydrodynamic tangent hyperbolic fluid flow past a stretching sheet, *Chinese J. Phys.*, **66** (2020), 258–268.

44. L. Ali, X. Liu, B. Ali, S. Mujeed, S. Abdal, S. A. Khan, Analysis of magnetic properties of nanoparticles due to a magnetic dipole in micropolar fluid flow over a stretching sheet, *Coatings*, **10** (2020), 170. https://doi.org/10.3390/coatings10020170

45. F. Ahmad, S. Abdal, H. Ayed, S. Hussain, S. Salim, A. O. Almatroud, The improved thermal efficiency of maxwell hybrid nanofluid comprising of graphene oxide plus silver/kerosene oil over stretching sheet, *Case Stud. Therm. Eng.*, **27** (2021), 101257.

46. B. K. Siddiqui, S. Batool, Q. M. ul Hassan, M. Malik, Irreversibility analysis in the boundary layer mhd two dimensional flow of maxwell nanofluid over a melting surface, *Ain Shams Engi. J.*, 2021. https://doi.org/10.1016/j.asej.2021.01.017

47. M. K. A. Mohamed, S. H. M. Yasin, M. Z. Salleh, H. T. Alkasasbeh, MHD stagnation point flow and heat transfer over a stretching sheet in a blood-based Casson ferrofluid with newtonian heating, *J. Adv. Res. Fluid Mech. Therm. Sci.*, **82** (2021), 1–11. https://doi.org/10.37934/arfmts.82.1.111

48. S. Abdal, B. Ali, S. Younas, L. Ali, A. Mariam, Thermo-diffusion and multislip effects on mhd mixed convection unsteady flow of micropolar nanofluid over a shrinking/stretching sheet with radiation in the presence of heat source, *Symmetry*, **12** (2020), 49. https://doi.org/10.3390/sym12010049

49. S. Abdal, I. Siddique, S. M. Eldin, M. Bilal, S. Hussain, Significance of thermal radiation and bioconvection for williamson nanofluid transportation owing to cone rotation, *Sci. Rep.*, **12** (2022), 22646.

50. I. S. U. Din, I. Siddique, R. Ali, F. Jarad, S. Abdal, S. Hussain, On heat and flow characteristics of carreau nanofluid and tangent hyperbolic nanofluid across a wedge with slip effects and bioconvection, *Case Stud. Therm. Eng.*, **39** (2022), 102390.

51. I. Siddique, U. Habib, R. Ali, S. Abdal, N. Salamat, Bioconvection attribution for effective thermal transportation of upper convicted maxwell nanofluid flow due to an extending cylindrical surface, *Int. Commun. Heat Mass*, **137** (2022), 106239. https://doi.org/10.1016/j.icheatmasstransfer.2022.106239

52. B. Ali, S. Hussain, M. Shafique, D. Habib, G. Rasool, Analyzing the interaction of hybrid base liquid $C_2H_6O_2$-H_2O with hybrid nano-material Ag-MoS_2 for unsteady rotational flow referred to an elongated surface using modified buongiorno's model: FEM simulation, *Math. Comput. Simul.*, **190** (2021), 57–74. https://doi.org/10.1016/j.matcom.2021.05.012

53. A. U. Yahya, N. Salamat, W. H. Huang, I. Siddique, S. Abdal, S. Hussain, Thermal charactristics for the flow of williamson hybrid nanofluid (MoS_2+ ZnO) based with engine oil over a streched sheet, *Case Stud. Therm. Eng.*, **26** (2021), 101196. https://doi.org/10.1016/j.csite.2021.101196

54. B. Ali, R. A. Naqvi, D. Hussain, O. M. Aldossary, S. Hussain, Magnetic rotating flow of a hybrid nano-materials Ag-MoS_2 and Go-MoS_2 in $C_2H_6O_2$-H_2O hybrid base fluid over an extending surface involving activation energy: FE simulation, *Mathematics*, **8** (2020), 1730. https://doi.org/10.3390/math8101730

55. A. U. Yahya, I. Siddique, F. Jarad, N. Salamat, S. Abdal, Y. Hamed, et al., On the enhancement of thermal transport of kerosene oil mixed TiO_2 and SiO_2 across riga wedge, *Case Stud. Therm. Eng.*, **34** (2022), 102025.

56. L. Ali, Y. J. Wu, B. Ali, S. Abdal, S. Hussain, The crucial features of aggregation in TiO_2-water nanofluid aligned of chemically comprising microorganisms: A FEM approach, *Comput. Math. Appl.*, **123** (2022), 241–251. https://doi.org/10.1016/j.camwa.2022.08.028

57. R. S. R. Gorla, I. Sidawi, Free convection on a vertical stretching surface with suction and blowing, *Appl. Sci. Res.*, **52** (1994), 247–257. https://doi.org/10.1007/BF00853952

58. W. Khan, I. Pop, Boundary-layer flow of a nanofluid past a stretching sheet, *Int. J. Heat Mass*, **53** (2010), 2477–2483. https://doi.org/10.1016/j.ijheatmasstransfer.2010.01.032

59. C. Wang, Free convection on a vertical stretching surface, *ZAMM-J. Appl. Math. Mech.*, **69** (1989), 418–420. https://doi.org/10.1002/zamm.19890691115

60. S. U. Devi, S. A. Devi, Heat transfer enhancement of Cu-Al_2O_3 water hybrid nanofluid flow over a stretching sheet, *J. Nigerian Math. Soc.*, **36** (2017), 419–433.